



Modulation of macrophages by a paeoniflorin-loaded hyaluronic acid-based hydrogel promotes diabetic wound healing



Hao Yang^{a,d}, Liu Song^{a,d}, Bingxue Sun^a, Di Chu^a, Leilei Yang^a, Meng Li^a, Huan Li^a, Yun Dai^b, Zhuo Yu^c, Jianfeng Guo^{a,*}

^a School of Pharmaceutical Sciences, Jilin University, Changchun, 130021, China

^b Laboratory of Cancer Precision Medicine, The First Hospital of Jilin University, Changchun, 130021, China

^c Department of Hepatopathy, Shuguang Hospital, Affiliated to Shanghai University of Traditional Chinese Medicine, Shanghai, 201203, China

ARTICLE INFO

Keywords:

Macrophage polarization
Hydrogel
Anti-inflammation
Angiogenesis
Regenerative medicine

ABSTRACT

The impaired wound healing in diabetes is a central concern of healthcare worldwide. However, current treatments often fail due to the complexity of diabetic wounds, and thus, emerging therapeutic approaches are needed. Macrophages, a prominent immune cell in the wound, play key roles in tissue repair and regeneration. Recent evidence has demonstrated that macrophages in diabetic wounds maintain a persistent proinflammatory phenotype that causes the failure of healing. Therefore, modulation of macrophages provides great promise for wound healing in diabetic patients. In this study, the potential of paeoniflorin (PF, a chemical compound derived from the herb *Paeonia lactiflora*) for the transition of macrophages from M1 (proinflammatory phenotype) to M2 (anti-inflammatory/prohealing phenotype) was confirmed using *ex vivo* and *in vivo* experimental approaches. A hydrogel based on high molecular weight hyaluronic acid (HA) was developed for local administration of PF in experimental diabetic mice with a full-thickness wound. The resultant formulation (HA-PF) was able to significantly promote cutaneous healing as compared to INTRASITE Gel (a commercial hydrogel wound dressing). This outcome was accompanied by the amelioration of inflammation, the improvement of angiogenesis, and re-epithelialization, and the deposition of collagen. Our study indicates the significant potential of HA-PF for clinical translation in diabetic wound healing.

1. Introduction

The wound healing proceeds efficiently after surgical incision, traumatic injury, and superficial burn. The healing process generally comprises four stages, including hemostasis, inflammation, proliferation, and maturation [1]. However, this process may be retarded by certain physiological conditions (e.g., ischemia, obesity, and diabetes); consequently, it is obstructed at one of the stages [2]. Diabetes is recognized as one of the leading causes of chronic (non-healing) wounds, and diabetic

wounds complicate medical care, increase treatment costs, and worsen the life quality of patients [3]. However, as the cellular and molecular mechanisms underlying diabetic wounds remain incompletely understood, current therapeutic strategies are limited.

The macrophage is a type of leukocyte (or white blood cell) of the immune system and exists as a heterogeneous population in different tissues [4]. The macrophage is generally classified into M1 (or M1-like; termed as classically activated macrophages) and M2 (or M2-like; termed as alternatively activated macrophages) [5]. Macrophages play

Abbreviations: Adipic acid dihydrazide, ADH; arginase 1, Arg-1; α -smooth muscle actin, α -SMA; bone marrow-derived macrophages, BMDMs; dimethyl sulfoxide, DMSO; fetal bovine serum, FBS; human umbilical vein endothelial cells, HUVECs; hyaluronic acid, HA; inducible nitric oxide synthase, iNOS; integrated optical density, IOD; interleukin-1 β , IL-1 β ; interleukin-10, IL-10; interferon- γ , IFN- γ ; lipopolysaccharide, LPS; macrophage colony-stimulating factor, M-CSF; N-(3-Dimethylaminopropyl)-N'-ethylcarbodiimide hydrochloride, EDC.HCl; paeoniflorin, PF; penicillin-streptomycin, P/S; phosphate-buffered saline, PBS; polyvinylidene difluoride, PVDF; scanning electron microscopy, SEM; signal transducer and activator of transcription, STAT; streptomycin, STZ; swelling ratio, SR; transforming growth factor- β , TGF- β ; tumor necrosis factor- α , TNF- α .

* Corresponding author.

E-mail address: jguo@jlu.edu.cn (J. Guo).

^d These authors made equal contributions to this work.

<https://doi.org/10.1016/j.mtbio.2021.100139>

Received 12 July 2021; Received in revised form 28 August 2021; Accepted 5 September 2021

Available online 21 September 2021

2590-0064/© 2021 The Author(s). Published by Elsevier Ltd. This is an open access article under the CC BY-NC-ND license (<http://creativecommons.org/licenses/by-nc-nd/4.0/>).

key roles in wound healing at different stages [6], in which the transition from M1 to M2 occurs [7], as follows: (1) M1 macrophages destroy foreign pathogens and clean dead tissues at the inflammation stage; (2) M1 macrophages are polarized into M2 at the proliferation stage, and M2 macrophages facilitate the formation of a new blood vessel and granulation tissue; (3) M2 macrophages activate fibroblasts, which will promote the deposition of collagens for the integrity of wound site at the maturation stage. Increasing evidence indicates that macrophages are persistently maintained with the M1 phenotype in diabetic wounds, which can significantly hinder the skin repair and regeneration [7]. Therefore, modulation of macrophages from M1 to M2 provides great promise for the improvement of diabetic wound healing [8].

Paeoniflorin (PF) is the major bioactive ingredient in the total glycoside of paeony extracted from *Paeonia lactiflora* roots [9]. It has been reported that PF exerts immunoregulatory functions in preclinical animal models of inflammatory disorders (e.g., rheumatoid arthritis, inflammatory bowel disease, psoriasis, and asthma) [10]. This may be attributed to the capacity of PF for controlling the activity of macrophages [11–16]. In this study, the potential of PF for the modulation of macrophages from M1 to M2 was confirmed using *ex vivo* and *in vivo* experimental approaches. Accordingly, a high molecular weight hyaluronic acid-based hydrogel was developed to facilitate the local administration of PF for healing efficacy in streptozocin-induced diabetic mice with a full-thickness wound.

2. Materials and methods

2.1. Materials

Sodium hyaluronate with a range of molecular weights ($M_w = 800$ – $1,000$, $1,300$ – $1,500$, and 1800 – $2,200$ kDa) was obtained from Bloomage Biotech, China. The other materials and reagents were purchased from Sigma-Aldrich unless mentioned otherwise.

2.2. Animals

C57BL/6J male mice (~6–7 weeks and ~20 g) were purchased from Changchun Yisi Experimental Animal Technology Co., Ltd. Animals were allowed to acclimate for at least one week in the housing facility before the experiment. Mice were maintained in a pathogen-free animal facility (5 animals per cage) under standard conditions (22 ± 2 °C under a 12 h light/dark cycle: lights on at 08:00). Animals received food and water freely. The experiments have been approved by the Animal Ethics Committee of Jilin University.

2.3. Cytotoxicity

L929 cells (mouse fibroblasts) were maintained in DMEM (high glucose; Corning) supplemented with 10% fetal bovine serum (FBS; Corning) and 1% penicillin-streptomycin (P/S) (TransGen Biotech, China). HUVECs (human umbilical vein endothelial cells) were maintained in RPMI-1640 (Corning) supplemented with 10% FBS and 1% P/S. Cells were maintained at 37 °C with 5% CO₂ and 95% relative humidity.

The L929 and HUVECs (2,000 per well) were seeded in 96-well plates under the normal growth conditions for 24 h. Subsequently, cells were added with PF ([c] = 1, 5, 10, 25, 50, 100, and 200 μM) and incubated under the normal growth conditions for one day. After incubation, cells were added with 150 μL fresh growth media and 15 μL MTT stock (5 mg/mL) and incubated for 4 h at 37 °C. The purple formazan products were dissolved by DMSO before measurement at 570 nm using a microplate reader.

2.4. Phenotype and function of macrophages

The bone marrow-derived macrophages (BMDMs) were harvested and prepared as previously reported [17]. Briefly, the bone marrow was flushed from the femurs of 4–6 week old C57BL/6J mice using ice-cold

phosphate-buffered saline (PBS; Corning) and passed through the 70 μm cell strainers (BD Falcon). Cells were collected by centrifugation at 1,200 rpm for 5 min. The red blood cells were lysed with 1 mL Red Blood Cell Lysis Buffer (Yeasen Biotech, China) for 1 min. After centrifugation at 1200 rpm for 5 min, cells were seeded in 24-well plates (2×10^5 per well) within DMEM (high glucose) supplemented with 10% FBS, 1% P/S, and 10 ng/mL M-CSF (Biolegend). After three days, cells were added with fresh DMEM (high glucose) supplemented with 10% FBS, 1% P/S, and 10 ng/mL M-CSF. After two days, cells were added with DMEM (high glucose) supplemented with 10% FBS, 1% P/S, 100 ng/mL LPS, and 20 ng/mL IFN-γ. After one day, cells were added with PF ([c] = 10, 25 and/or 50 μM) for 24 h prior to the following experiments: (1) Flow cytometry [18]. The antigen expression was detected by fluorophore-labeled antibodies (Table S1) using BD FACSCalibur (Becton Dickinson). (2) RT-qPCR [19]. First-strand cDNA was generated using the TransScript® First-Strand cDNA Synthesis SuperMix kit (TransGen Biotech, China). RT-qPCR was carried out with TransStart® Top Green qPCR SuperMix kit (TransGen Biotech, China) using StepOnePlus™ Real-Time PCR System (ThermoFisher). The primers were listed in Table S2. (3) Western blot. The total protein was collected using the RIPA Lysis Buffer (GenStar, China) containing 1 mM PMSF (GenStar, China). The protein concentration was determined using the BCA kit (TransGen Biotech, China), and ~30 μg protein per sample was loaded onto an SDS-polyacrylamide gel and electrophoresed at 80–100 V for 1–2 h. Protein was transferred to a polyvinylidene difluoride (PVDF) membrane (Millipore) for 1–1.5 h at 200 mA. Membranes were incubated overnight with primary antibodies (Table S1) at 4 °C. The appropriate secondary antibodies (Table S1) were added to the membrane at room temperature for 1 h. Proteins were detected using the enhanced chemiluminescence solution (GE Healthcare). Quantification of proteins was carried out using densitometry (ImageJ), and all results were normalized to β-Actin. (4) ELISA. The level of cytokines in the supernatant was assessed using mouse TNF-α, IL-1β, IL-10, and TGF-β ELISA kits (LanpaiBIO Co., Ltd., China).

2.5. Preparation, physicochemical characterization, and *in vivo* performance of hyaluronic acid hydrogels

For preparing the crosslinked hydrogels, the sodium hyaluronate was dissolved in deionized water ([c] = 0.4 μM) at 50–55 °C with stirring. This solution was added with ADH ([c] = 15 mM) at room temperature with stirring, and the pH was adjusted to ~4.5 to 4.7 prior to the addition of EDC. HCl ([c] = 0.5 mM). Following vigorous stirring, the solution became gelatinous due to the formation of crosslinked hydrogels. The hydrogels were washed with PBS (pH = 7.4) and subsequently washed using pure ethanol with sonication. The hydrogels were air-dried, rehydrated using deionized water, and dried using a freezer-drier for long-term storage.

The physicochemical property of hydrogels was assessed as follows: (1) Morphology [20]. The structure of dried hydrogels was observed using scanning electron microscopy (SEM). (2) Swelling ratio (SR) [21]. Dried hydrogels (0.05 g) were incubated in PBS (pH = 7.4), the swelled hydrogels were collected, and the water was removed from the surface of hydrogels until the weight was not changed. The SR was calculated as $SR = (W_s - W_d) / W_d$, where W_s = the weight of hydrogels at the swelling state and W_d = the weight of hydrogels at the dry state. (3) Enzymolysis resistance [22]. Dried hydrogels (0.05 g) were completely rehydrated based on SR determined as above and subsequently placed in 1 mL hyaluronidase solution (100 U/mL). Following the incubation at 0, 24 and 48 h, 0.2 mL samples were added into 1.2 mL sulfuric acid. After heating at 95–100 °C for 10 min, the content was added with 0.1 mL carbazole solution (0.15% W/V in absolute ethanol) prior to the measurement at the absorbance of 530 nm using the microplate reader. (4) Release rate [23]. Dried HA (0.05 g) was incubated with 10 mL of BSA solution (10 mg/mL) to produce BSA-loaded hydrogels. The hydrogels were removed, and the amount of BSA left in the solution was determined using NanoDrop™ (Thermo Scientific). The amount of BSA inside hydrogels = (the feed amount) - (the amount of BSA left in the solution).

Subsequently, BSA-loaded hydrogels were incubated in 2 mL PBS (pH = 7.4) at 37 °C with gentle shaking. The amount of BSA released from hydrogels into the solution at different time points was measured using NanoDrop™ to determine the release rate.

Two full-thickness wounds (~0.3 cm²) per animal were made using disinfected surgical scissors deeply into the dermis without disturbing the subdermal vasculature on the dorsal surface. On days 0, 2, and 4, the wounds were randomly grouped, and were treated with 100 μL of hydrogels (4%, 8%, and 12%, W/V in PBS). The wound diameter was recorded on days 0, 3, 7, and 14. The wound healing rate was calculated as $(1 - S_n/S_0) \times 100\%$, where S_n = the wound surface area at a pre-determined day and S_0 = the wound surface area at day 0.

2.6. The wound healing efficacy of paeoniflorin-loaded hydrogel in diabetic mice

Experimental diabetic mice were established as previously reported [24]. Briefly, streptozocin (STZ) was freshly prepared at a concentration of 20% (W/V) in sodium citrate buffer solution (pH = 4.5). Mice were intraperitoneally injected with STZ solution at a dose of 55 mg/kg for 5 days. Subsequently, the blood was collected from the tail, and the concentration of glucose in the blood was measured using a blood glucose meter. The mice with blood glucose more than 14 mmol/L were considered as diabetic mice [24,25], and the full-thickness wound was established as described above. Subsequently, animals were randomly grouped, and the blood glucose was measured throughout the experiment to ensure a concentration of glucose of more than 14 mmol/L. In order to prepare PF-loaded hydrogels (HA-PF), PF was dissolved in propylene glycol ([c] = 25,000, 50,000, 100,000 and 200,000 μM), and was diluted in PBS (pH = 7.4) ([c] = 250, 500, 1,000 and 2,000 μM) to achieve the PF solutions. Subsequently, 1 mL of PF solutions were added to 0.08 g of dried HA (prepared as described above), achieving HA-PF (8% hydrogels; the PF solutions were fully absorbed by dried HA at this condition; theoretically, PF was fully loaded into hydrogels). The healing efficacy of 100 μL HA-PF was assessed as described above. In addition, 100 μL blank hydrogel and 100 μL INTRASITE Gel were used as controls.

At predetermined days, the wound specimen without surrounding healthy tissues was obtained for the following experiments: (1) Hematoxylin-eosin (H&E) staining assay [26]. The samples were fixed in 4% paraformaldehyde, embedded in paraffin, and sectioned (5 μm). Sections were used for H&E staining, and the inflammatory cell infiltration, fibroblast proliferation, and blood vessel formation were observed under the microscope (Olympus BX53). The number (N) of positive cells and the area (a) in the slide were analyzed using Image-Pro Plus 6.0 software (Media Cybernetics, Inc., USA). The level of inflammatory cell infiltration with the treatment of blank hydrogel, INTRASITE Gel, and HA-PF was determined as N/a corrected according to the untreated group. In addition, three areas of the epidermis layer in the slide were randomly selected to measure the mean of epidermal thickness using Image-Pro Plus 6.0 software. The level of fibroblast proliferation with the treatment of blank hydrogel, INTRASITE Gel, and HA-PF was determined as the mean of epidermal thickness corrected according to the untreated group. Moreover, the development of blood vessels was quantified based on the mean of new blood vessels in the slide. (2) Masson's trichrome staining assay. The collagen deposition was observed under the microscope (Olympus BX53). The collagen area (%), also known as collagen volume fraction (CVF; it is the percentage of the blue area positive for collagen relative to the total tissue area) in the slide, was analyzed using Image-Pro Plus 6.0 software (Media Cybernetics, Inc., USA). The quantitative level in collagen deposition with the treatment of blank hydrogel, INTRASITE Gel, and HA-PF was determined as the CVF corrected according to the untreated group. (3) Immunofluorescent staining assay [27]. The dewaxed sections were followed by the retrieval of antigen, permeabilization, and blocking in 5% BSA. Slides were incubated with primary antibodies (Table S1) overnight at 4 °C, followed by incubation with secondary antibodies (Table S1). After

the nucleus staining with DAPI (Beyotime Biotech, China), slides were observed under the confocal microscope (Olympus FV3000). (4) RT-qPCR. The samples were homogenized with TriZol Up reagent (TransGen Biotech, China) using a tissue grinder (Scientz, China). The homogenates were centrifuged at 12,500 rpm for 20 min at 4 °C, and the total RNA was collected from the supernatant using TransZol UP (TransGen Biotech, China). RT-PCR was performed as described above. The primers were listed in Table S2. (5) ELISA [28]. The samples were homogenized within the RIPA Lysis Buffer containing 1 mM PMSF using the tissue grinder. The homogenates were centrifuged at 12,500 rpm for 20 min at 4 °C to collect the total protein. The level of proteins in the content was assessed using mouse TNF-α, IL-1β, IL-10, and TGF-β ELISA kits (LanpaiBIO Co., Ltd., China).

2.7. Statistical analysis

Results were presented as the mean ± standard deviation (SD) (n = sample size). A two-way ANOVA (Bonferroni's Post-Hoc test) was used to test the significance of differences. In all experiments, $p < 0.05$ was considered statistically significant.

3. Results

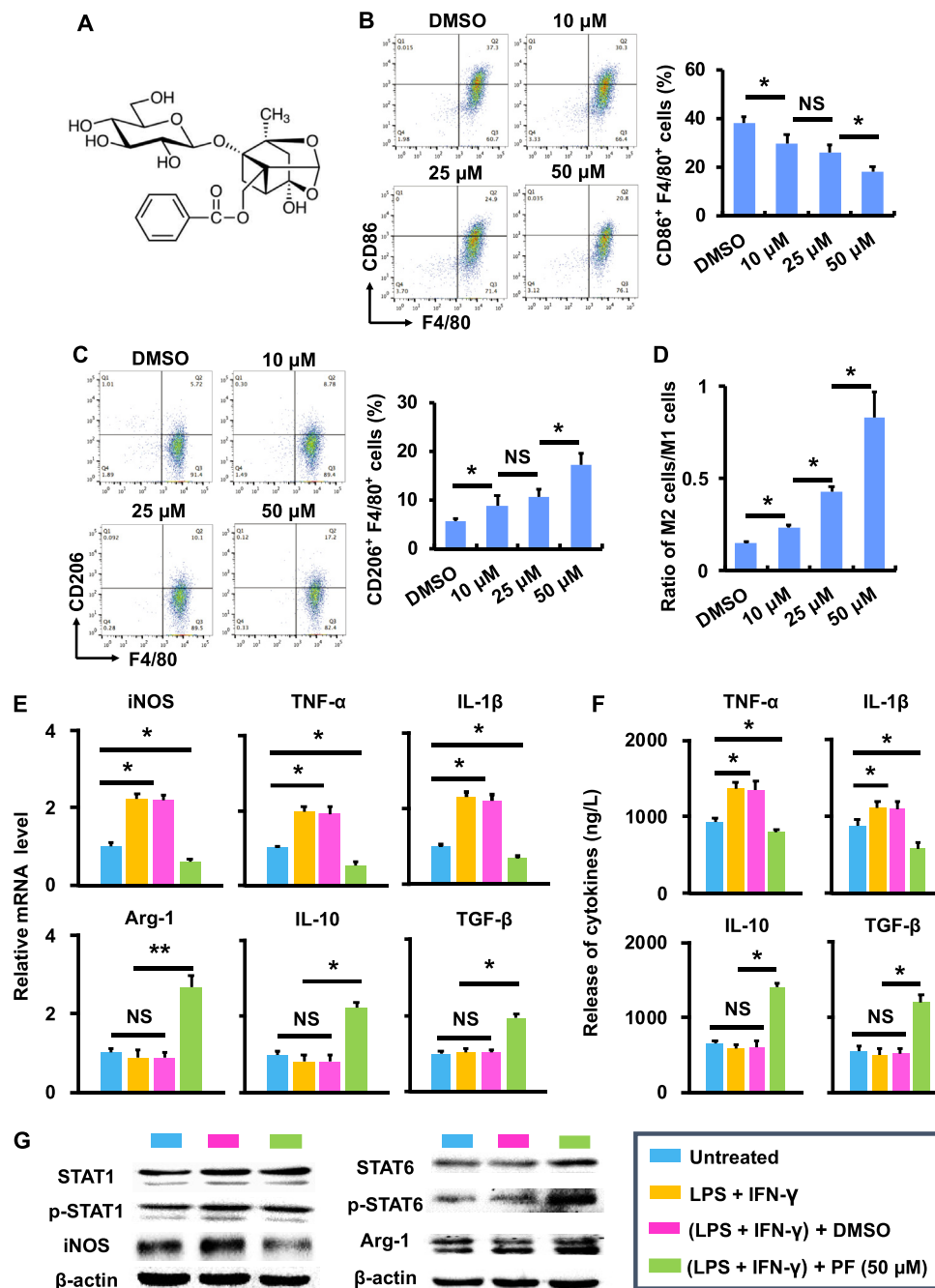
3.1. Paeoniflorin modulates the phenotype and function of macrophages

The cytotoxicity of paeoniflorin (PF; Fig. 1A) was assessed in mouse fibroblasts (L929) and human umbilical vein endothelial cells (HUVECs) using the MTT assay, respectively (Fig. S1). Results show that no significant cytotoxicity was caused by PF in two cell lines under the concentrations tested (up to 200 μM) (Fig. S1). The potential of PF to modulate the phenotype and function of macrophages was subsequently assessed using BMDMs. BMDMs were polarized into M1 following the stimulation of LPS and IFN-γ [29], and the polarization was confirmed by the expression of CD86 and F4/80 (two commonly used phenotypic markers for M1 macrophages) using flow cytometry (dot plot). As shown in Fig. 1B and S2, the number of CD86- and F4/80-expressing cells was significantly ($p < 0.05$) reduced following the treatment of PF ([c] = 10, 25, and 50 μM) as compared to the DMSO group. In contrast, the number of cells with the expression of CD206 and F4/80 (two commonly used phenotypic markers for M2 macrophages) was significantly ($p < 0.05$) increased following the treatment of PF as compared to the DMSO group at the same concentrations (analyzed using flow cytometry, dot plot; Fig. 1C and S2). Consequently, the ratio of M2 versus M1 was significantly ($p < 0.05$) increased by PF (Fig. 1D), indicating the role of PF in modulating the phenotype of macrophages from M1 (or M1 like) to M2 (or M2 like).

In addition to phenotypic modulation, PF was able to control the function of macrophages. As shown in Fig. 1E, the mRNA level of iNOS, TNF-α, and IL-1β (three functional markers associated with M1 macrophages) produced by LPS- and IFN-γ-stimulated BMDMs was significantly ($p < 0.05$) reduced by PF, while the mRNA level of Arg-1, IL-10, and TGF-β (three functional markers associated with M2 macrophages) were significantly ($p < 0.05$) increased by PF. In addition, the release of TNF-α and IL-1β was significantly ($p < 0.05$) suppressed by PF, while the release of IL-10 and TGF-β was significantly ($p < 0.05$) enhanced by PF (Fig. 1F).

The capacity of PF in regulating the signal transducer and activator of transcription (STAT) signaling pathway (a classic pathway underlying macrophage polarization) was assessed using LPS- and IFN-γ-stimulated BMDMs. Results show that STAT1 (a key protein associated with M1 macrophages) was significantly ($p < 0.05$) deactivated by PF, while STAT6 (a key protein associated with M2 macrophages) was significantly ($p < 0.05$) activated by PF (Fig. 1G and S3). Consequently, the expression of iNOS, a downstream protein of STAT1, was significantly ($p < 0.05$) suppressed, while the expression of Arg-1, a downstream protein of STAT6, was significantly ($p < 0.05$) enhanced (Fig. 1G and S3).

Fig. 1. Paeoniflorin modulates the phenotype and function of macrophages. (A) The chemical structure of paeoniflorin (PF). (B) The CD86⁺ and F4/80⁺ population (%) in LPS- and IFN- γ -stimulated BMDMs following treatment of DMSO and PF (10, 25 and 50 μ M) (n = 3; *p < 0.05 and NS = no significance). (C) The CD206⁺ and F4/80⁺ population (%) in LPS- and IFN- γ -stimulated BMDMs following treatment of DMSO and PF (10, 25 and 50 μ M) (n = 3; *p < 0.05 and NS = no significance). (D) The ratio of M2 cells (CD206⁺ and F4/80⁺) versus M1 cells (CD86⁺ and F4/80⁺) (n = 3; *p < 0.05 and NS = no significance). (E) The mRNA expression of cytokines in LPS- and IFN- γ -stimulated BMDMs following treatment of DMSO and PF (50 μ M) (n = 3; *p < 0.05 and NS = no significance). (F) The release of cytokines in LPS- and IFN- γ -stimulated BMDMs following treatment of DMSO and PF (50 μ M) (n = 3; *p < 0.05 and NS = no significance). (G) The activity of STAT signaling pathway in LPS- and IFN- γ -stimulated BMDMs following treatment of DMSO and PF (50 μ M). The relative expression of the proteins of interest was quantified in Fig. S3.



3.2. Preparation, physicochemical characterization, and *in vivo* performance of hyaluronic acid hydrogels

Subsequently, a hydrogel based on high molecular weight hyaluronic acid (HA) was developed to facilitate *in vivo* application of PF (Fig. 2). As shown in Fig. 2A, hydrogels were produced by crosslinking a range of HA polymers (*M_w* = 800–1,000, 1,300–1,500, and 1,800–2,200 kDa) *via* ADH. The SEM results show that crosslinked HAs presented a porous 3-dimensional (3D) morphology, whereas non-crosslinked HAs displayed an irregular 2D structure (Fig. 2B). In addition, the physicochemical property of crosslinked HAs was evaluated in terms of swelling rate (Fig. 2C), enzymatic hydrolysis resistance (Fig. 2D), and sustained-release rate (Fig. 2E). Results show that the crosslinked HA with *M_w* of 1,800–2,200 kDa significantly improved the swelling capacity, enhanced

the enzymatic hydrolysis resistance, and facilitated long-term drug release, in comparison to the counterparts with *M_w* of 800–1,000 and 1,300–1,500 kDa. Therefore, the crosslinked HA with *M_w* of 1,800–2,200 kDa was selected for the following *in vivo* experiments.

The fluidity of hydrogels was decreased with the increment of the concentration (Fig. 2F); when the concentration was increased to 12%, the hydrogel became condensed (Fig. 2F). It has been reported that HA as a hydrogel dressing may improve wound healing [30]. In this study, crosslinked hydrogels with the concentration of 4%, 8%, and 12% were applied to mice with a full-thickness wound (Fig. 2G). Results show that the 8% hydrogel accelerated the wound closure as compared to 4% and 12% counterparts. This is likely due to the fact that 8% hydrogel achieved a favorable viscosity for local administration. Therefore, the hydrogel was prepared using 1,800–2,200 kDa of crosslinked HA at a

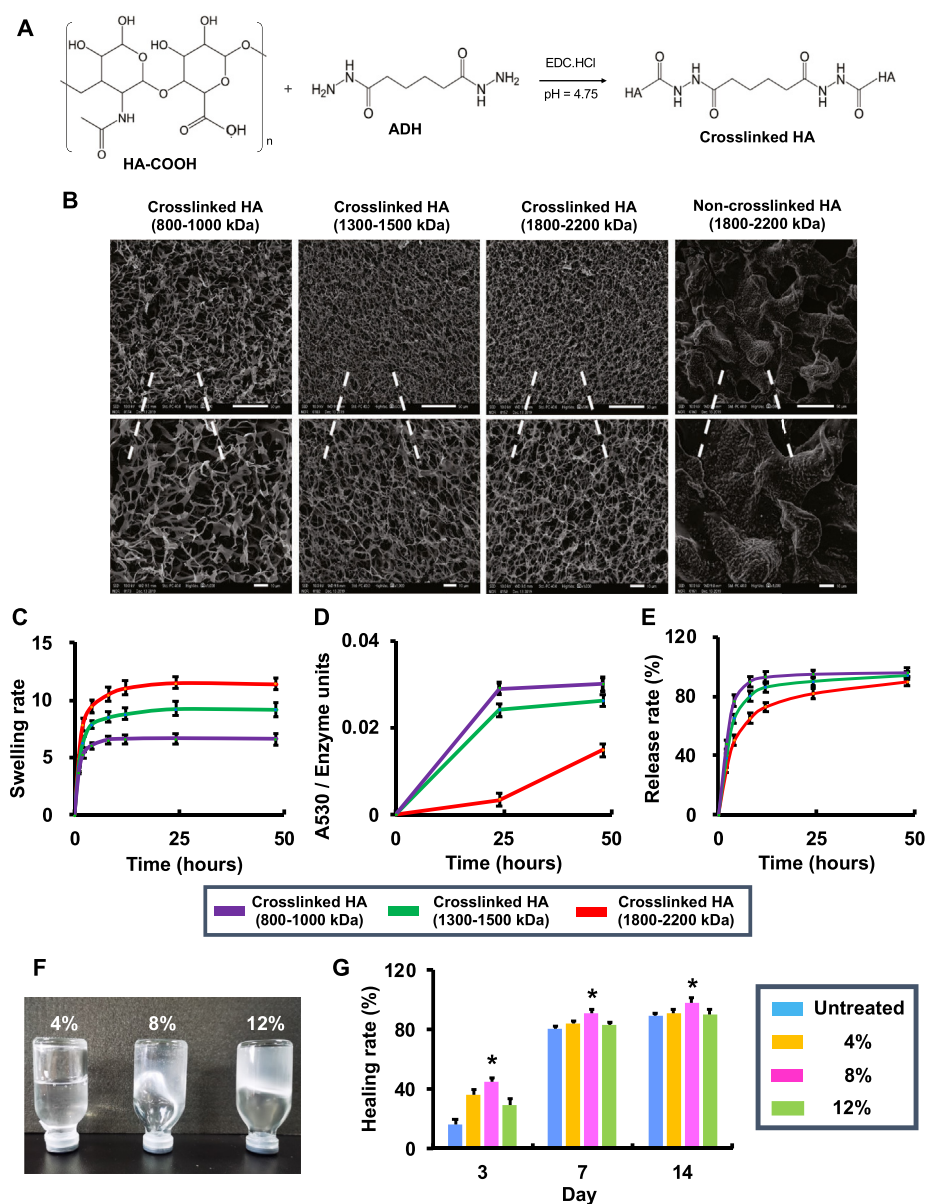


Fig. 2. Preparation, physicochemical characterization, and *in vivo* performance of hyaluronic acid hydrogels. (A) The schematic for preparation of crosslinked HA. (B) SEM image of crosslinked HA with different molecular weights (M_w) (bar in the upper lane = 50 μm and bar in the lower lane = 10 μm). (C) The swelling rate of crosslinked HA with different M_w ($n = 3$). (D) The enzymatic hydrolysis resistance of crosslinked HA with different M_w ($n = 3$). (E) The release rate of BSA in crosslinked HA with different M_w ($n = 3$). (F) The images of crosslinked hydrogels ($M_w = 1,800\text{--}2,200$ kDa) at the concentration of 4%, 8% and 12%. (G) The healing rate (%) of mice with full-thickness wounds following treatment of crosslinked hydrogels ($M_w = 1,800\text{--}2,200$ kDa) at the concentration of 4%, 8% and 12% ($n = 4$; * $p < 0.05$ relative to untreated, 4% and 12%).

concentration of 8% for local administration of PF in diabetic wound healing (Fig. 3).

3.3. Paeoniflorin-loaded hydrogel accelerates diabetic wound closure in mice

In order to optimize the dose of PF for *in vivo* application, the hydrogels containing PF (referred to as HA-PF) at the dose of 250, 500, 1,000, and 2,000 μM were locally administrated to experimental diabetic mice with a full-thickness wound (Fig. S4). Results show that the wound healing was significantly ($p < 0.05$) improved by HA-PF relative to the untreated group (Fig. S4). In addition, HA-PF demonstrated sustained release of PF (Fig. S5), which was similar to the results described in Fig. 2E. Due to the effective wound healing achieved by HA-PF at 500 μM of PF, this dose was selected for the following experiments.

The experimental diabetic mice with full-thickness wounds were established as described in Fig. 3A and S6. On day 0, the blank hydrogel, INTRASITE Gel (a commercial hydrogel wound dressing), and HA-PF were locally applied to diabetic wounds. Results show that the blank hydrogel and INTRASITE Gel significantly ($p < 0.05$) improved wound healing as compared to the untreated group on days 3, 7, and 14, while

HA-PF was able to further ($p < 0.05$) accelerate the wound closure relative to the blank hydrogel and INTRASITE Gel (Fig. 3B). Consequently, the reduction of inflammatory infiltration, amelioration of epidermal hyperplasia, and enhancement of new blood vessel growth (angiogenesis) were significantly ($p < 0.05$) achieved by HA-PF relative to the blank hydrogel and INTRASITE Gel on day 14 (Fig. 3C). In addition, the collagen disposition was significantly ($p < 0.05$) improved by HA-PF relative to the controls on day 14 (Fig. 3D). These results indicate that HA-PF could promote diabetic wound healing via the suppression of inflammatory infiltration and epidermal hyperplasia, and the improvement of angiogenesis and collagen disposition.

3.4. Healing effects of paeoniflorin-loaded hydrogel

Due to *ex vivo* effects achieved by PF (Fig. 1), the capacity of HA-PF for diabetic wound healing based on the modulation of macrophages was also confirmed *in vivo* (Fig. 4). Immunofluorescent results show that the blank hydrogel and INTRASITE Gel could not significantly change the population of M1 phenotype (iNOS^+ and F4/80^+) out of the total macrophages as compared to the untreated control on day 7, while HA-PF significantly ($p < 0.05$) reduced the population of M1 phenotype

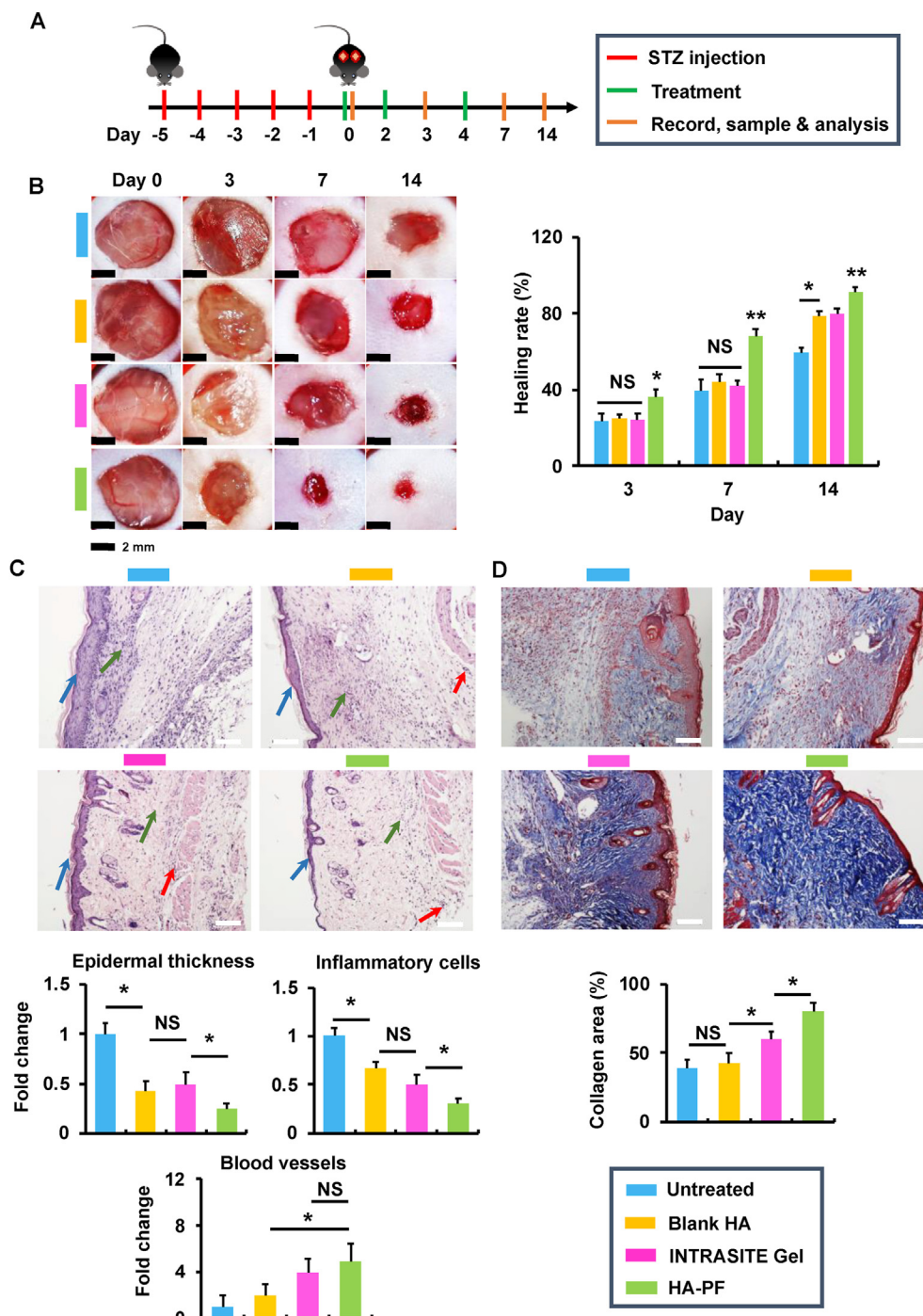


Fig. 3. Paeoniflorin-loaded hydrogel accelerates diabetic wound closure in mice. (A) The treatment schematic for STZ-induced diabetic mice with full-thickness wounds. (B) Images of incisional wounds after treatments of blank HA, INTRASITE gel, and HA-PF (containing 500 μ M of PF). Healing rate (%) when compared with the wound area on day 0 (n = 8). The level of blood glucose in mice was monitored to ensure the formation of diabetes during the experiments (Fig. S4). (C) In H&E staining images (white bar = 20 μ m), the blue, green and red arrows represent epidermal hyperplasia, proinflammatory cells, and new blood vessels, respectively (n = 6; * p < 0.05 and NS = no significance). (D) In Masson's trichrome staining images (white bar = 20 μ m) (red = keratin, muscle fibers or cytoplasm, blue = collagen), the collagen deposition was quantified (n = 6; * p < 0.05 and NS = no significance).

relative to the blank hydrogel and INTRASITE Gel (Fig. 4A). In addition, the blank hydrogel and INTRASITE Gel could not significantly change the population of M2 phenotype (CD206⁺ and F4/80⁺) out of the total macrophages as compared to untreated control on day 7, while HA-PF significantly (p < 0.05) increased the population of M2 phenotype relative to the blank hydrogel and INTRASITE Gel (Fig. 4A). This was accompanied by the downregulation of proinflammatory factors (iNOS, TNF- α , and IL-1 β) and the upregulation of anti-inflammatory/prohealing factors (Arg-1, IL-10, and TGF- β) on day 7 (Fig. 4B and C).

The improvement of M2 macrophages achieved by HA-PF significantly (p < 0.05) enhanced the expression of CD31 and VEGF as compared to the blank hydrogel and INTRASITE Gel on day 14 (Fig. 4D). Immunofluorescent results further confirm that the expression of CD31

was significantly (p < 0.05) improved by HA-PF on day 14 (Fig. 4E). In addition, the improvement of M2 macrophages achieved by HA-PF also significantly (p < 0.05) promoted the expression of α -SMA and type I collagen as compared to the blank hydrogel and INTRASITE Gel at day 14 (Fig. 4D). Immunofluorescent results also confirm that the expression of α -SMA was significantly (p < 0.05) enhanced by HA-PF on day 14 (Fig. 4F). In addition, the enhanced expression of type I collagen achieved by HA-PF was compliant with the collagen disposition, as shown in Fig. 3D. These results indicate that HA-PF could modulate macrophages, which achieved the amelioration of inflammation, the improvement of angiogenesis and re-epithelialization, and the enhancement of collagen deposition, resulting in the improvement of diabetic wound healing.

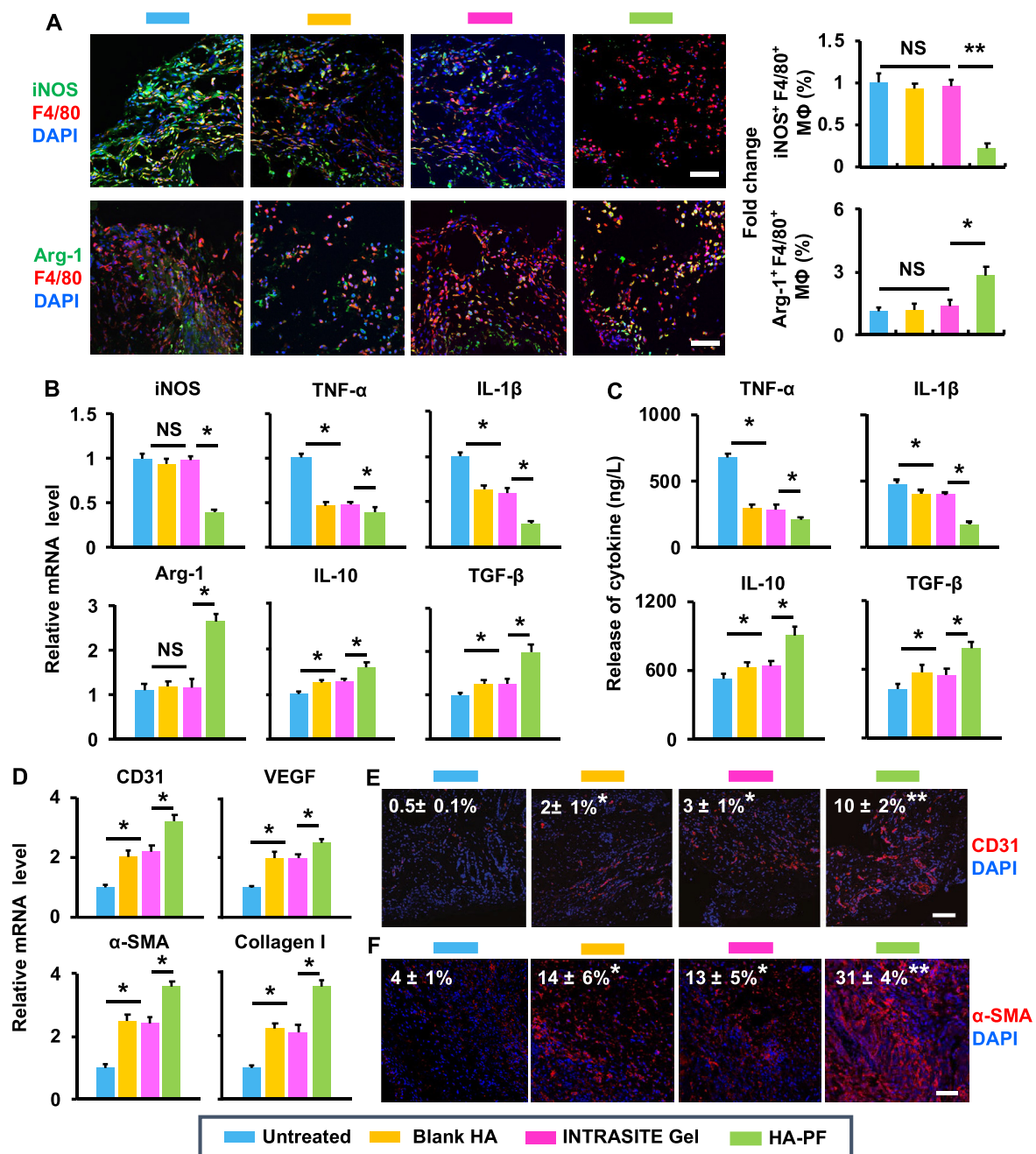


Fig. 4. HA-PF promotes diabetic wound healing via modulation of macrophages. (A) The population (%) of iNOS⁺ F4/80⁺ and Arg-1⁺ F4/80⁺ macrophages within the wound was determined using immunofluorescent assay (n = 4; *p < 0.05 and NS = no significance). (B) The mRNA expression of cytokines in the wound following treatment of blank HA, INTRASITE gel, and HA-PF (containing 500 μM of PF) (n = 4; *p < 0.05 and NS = no significance). (C) The release of cytokines in the wound following different treatments (n = 4; *p < 0.05). (D) The mRNA expression of CD31, VEGF, α-SMA and type I collagen in the wound following different treatments (n = 4; *p < 0.05 and NS = no significance). (E) The expression of CD31 in the wound was determined using immunofluorescent assay (n = 4; *p < 0.05 and NS = no significance). (F) The expression of α-SMA in the wound was determined using immunofluorescent assay (n = 4; *p < 0.05 and NS = no significance).

4. Discussion

Wound healing is generally composed of four stages, including hemostasis, inflammation, proliferation, and maturation [31]. Hemostasis occurs immediately after a lesion, which will stop bleeding from injured blood vessels in seconds (up to hours). The inflammatory stage is induced by proinflammatory factors for killing the invading pathogens and cleaning the dead tissues. Subsequently, the epithelial closure (re-epithelialization) and new blood vessel formation (angiogenesis) are accomplished in the proliferation stage. Finally, the newly formed tissues

are reorganized to enhance the integrity of the wound site at the maturation stage. Emerging evidence shows that a variety of cell types are involved in the wound healing [32]. Among these, macrophages play key roles at different stages of wound healing [33]. For example, M1 (or M1-like) macrophages produce proinflammatory factors and reactive oxygen/nitrogen species for controlling the infection at the early inflammation stage, while M2 (or M2-like) counterparts produce anti-inflammatory factors for the resolution of the inflammation stage [34]. In addition, M2 (or M2-like) macrophages produce growth factors for promoting the re-epithelialization, angiogenesis, and collagen

disposition during the proliferation and maturation stages [7].

It has become increasingly clear that the failure in the transition of macrophages from proinflammatory to anti-inflammatory/prohealing causes impaired diabetic wound healing [35]. It has been reported that the local administration of insulin changed the polarization of macrophages from M1 to M2, which restored the inflammatory response, resulting in acceleration of diabetic wound healing [36]. In addition, the local treatment of IL-33 (an inducer of Th2 type immunity) amplified the polarization of macrophages into M2 phenotype, which enhanced the proliferation of fibroblasts and the formation of new blood vessels, promoting wound healing in diabetic mice [37]. These imply that the modulation of macrophages provides the promise for treating diabetic wounds.

Recently, PF has demonstrated the potential of treating inflammatory disorders, which is likely due to the capacity for orchestrating the activity of macrophages [11–16]. In this study, PF was able to reduce the population of CD86- and F4/80-expressing macrophages and increase the population of CD206- and F4/80-expressing macrophages (Fig. 1B to D), indicating the capacity of PF for modulating the phenotype of macrophages from M1 to M2. In addition, PF could suppress the production of proinflammatory factors (iNOS, TNF- α , and IL-1 β) and enhance the production of anti-inflammatory/prohealing factors (Arg-1, IL-10, and TGF- β) (Fig. 1E and F), demonstrating the capacity of PF for modulating the function of macrophages from proinflammatory to anti-inflammatory/prohealing. Furthermore, PF could deactivate STAT1 (a key protein associated with M1 macrophages) but activate STAT6 (a key protein associated with M2 macrophages) (Fig. 1G and S3), indicating that PF could modulate the phenotype and function of macrophages via the regulation of STAT signaling pathway. Therefore, the results of Fig. 1 indicate the potential of PF for promoting diabetic wound healing via modulation of macrophages.

Recently, a variety of materials and techniques have been developed for biomedical applications [38–41]. Among these, HA, as a glycosaminoglycan of the extracellular matrix, plays a critical role in tissue repair and regeneration [42]. Recent advances in polymerization approaches have facilitated the development of HA derivatives as reparative biomaterials for wound healing [43]. In addition, HA-based hydrogel systems have been developed to deliver therapeutic agents (e.g., growth factors) [44] and living cells (e.g., human microvascular endothelial cells and fibroblasts) [45] for wound healing. For facilitating *in vivo* application of PF, hydrogels were produced in this study by crosslinking high molecular weight HA polymers with ADH (Fig. 2A). The crosslinked HAs demonstrated a porous 3D morphology (Fig. 2B), indicating the potential for loading of PF. In addition, the crosslinked HA ($M_w = 1,800$ –2,

200 kDa) significantly improved the physicochemical performance relative to counterparts ($M_w = 800$ –1,000 and 1,300–1,500 kDa) in terms of the swelling rate, enzymatic hydrolysis resistance, and sustained-release rate (Fig. 2C to E). These suggest that the crosslinked HA ($M_w = 1,800$ –2,200 kDa) facilitates the high loading and long-term release of PF. In addition, when this hydrogel on its own was locally administrated to the wounds, the healing efficacy was significantly improved relative to untreated control (Fig. 2G). Notably, the wound closure was significantly accelerated by 8% hydrogel, which is likely due to the appropriate viscosity as compared to the other counterparts (Fig. 2F). Therefore, the results of Fig. 2 indicate the potential of HA-based hydrogel as the delivery system for local administration of PF in treating diabetic wound healing.

The local application of HA-PF at the dose of 500 μ M PF could significantly promote diabetic wound healing (Fig. 3B). The wound healing was accompanied by the suppression of inflammatory infiltration and epidermal hyperplasia (fibroblast proliferation), and the improvement of angiogenesis and collagen disposition (Fig. 3C and D), indicating the capacity of HA-PF for fulfilling the inflammation, proliferation, and maturation stages. This outcome was mainly due to the capacity of HA-PF to improve M2 macrophages for anti-inflammation/prohealing (Fig. 4). HA-PF significantly ($p < 0.05$) reduced the population of M1 macrophages but significantly ($p < 0.05$) elevated the population of M2 macrophages inside the wound on day 7 postinjury (Fig. 4A), indicating that HA-PF was able to facilitate the polarization of macrophages from M1 to M2 at the late inflammation stage. The macrophage polarization resulted in the resolution of inflammation, which was evident with the down-regulation of iNOS, TNF- α , and IL-1 β and the upregulation of Arg-1, IL-10, and TGF- β (Fig. 4B and C). It has been reported that M2 macrophages produce growth factors (e.g., TGF- β and VEGF) for stimulating the activation of vascular cells and fibroblasts [46]. Indeed, HA-PF significantly ($p < 0.05$) improved the expression of CD31 (a marker for neovascularization), VEGF (a growth factor for angiogenesis), α -SMA (a marker for myofibroblast formation), and type I collagen (the most abundant collagen in the skin) on day 14 after injury (Fig. 4D to F). This indicates the role of HA-PF in promoting angiogenesis, re-epithelialization, and collagen disposition at the proliferation and maturation stages. These results confirm that modulation of macrophages by the local administration of HA-PF promoted diabetic wound healing. In addition, it is worth noting that HA-PF was able to significantly improve the healing efficacy relative to INTRASITE Gel (a commercial hydrogel wound dressing) (Figs. 3 and 4). This provides a great promise of HA-PF for clinical translation in diabetic wound healing.

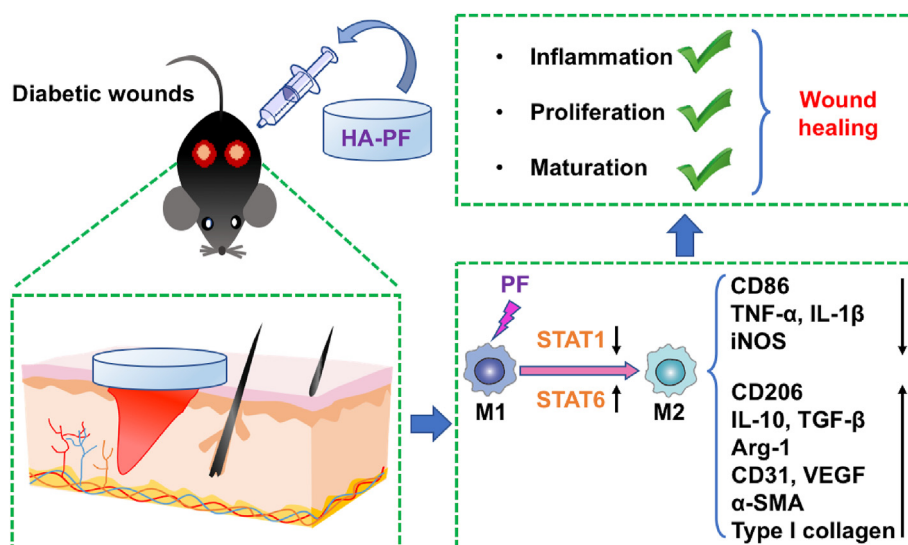


Fig. 5. Modulation of macrophages by a paeoniflorin-loaded hyaluronic acid-based hydrogel (HA-PF) promotes diabetic wound healing.

5. Conclusions

Accumulated evidence shows that the dysregulation of macrophages may cause impaired wound healing in diabetes [47]. In this study, a PF-loaded HA-based hydrogel system (namely HA-PF) has been developed for orchestrating the phenotype and function of macrophages in diabetic wounds (Fig. 5). Consequently, HA-PF successfully achieved the PF-mediated transition of macrophages from M1 (proinflammatory) to M2 (anti-inflammatory and prohealing), resulting in the promotion of diabetic wound healing. It should be borne in mind that although macrophages are generally classified into M1 and M2, the heterogeneity and plasticity of macrophages have not been fully characterized [48]. Therefore, the role of HA-PF in the phenotypic and functional switch of macrophage subpopulations associated with diabetic wounds will be further investigated in the future. It is also worth noting that a multimodal strategy is highly required for the treatment of diabetic wounds [49]. Therefore, HA-PF as regenerative medicine may be used in combination with other strategies that can control hyperglycemia and secondary infection in order to improve therapeutic outcomes for diabetic wounds.

Data availability statement

Data are available upon reasonable request.

Credit author statement

H.Y. and L.S. have performed data curation, methodology, formal analysis, and writing - original draft. B.S., D.C., L.Y., M.L., and H.L. have performed validation and formal analysis. H.L., Y.D., and Z.Y. have performed writing - review and editing. Z.Y. has provided resources and funding acquisition. J.G. has provided conceptualization, supervision, writing - review and editing, and funding acquisition.

Declaration of competing interest

The authors declare that they have no known competing financial interests or personal relationships that could have appeared to influence the work reported in this paper.

Acknowledgments

The authors would like to thank Mr. Bo Sun for his assistance in preparing the H&E and Masson's trichrome staining assays. This work was supported by the Health Commission of Jilin Province, China (2020Q012, to J.G.), the Department of Education of Jilin Province, China (JJKH20190099KJ, to J.G.), the Outstanding Youth Foundation from the Department of Science and Technology of Jilin Province, China (20170520046JH, to J.G.), the Fundamental Research Funds for the

Central Universities, China (to J.G.), and the National Natural Science Foundation of China, China (81774240, 82074154, to Z.Y.).

Appendix A. Supplementary data

Supplementary data to this article can be found online at <https://doi.org/10.1016/j.mtbio.2021.100139>.

References

- [1] G.C. Gurtner, et al., *Nature* 453 (7193) (2008) 314.
- [2] S. Guo, L.A. DiPietro, *J. Dent. Res.* 89 (3) (2010) 219.
- [3] D. Baltzis, et al., *Adv. Ther.* 31 (8) (2014) 817.
- [4] S. Gordon, P.R. Taylor, *Nat. Rev. Immunol.* 5 (12) (2005) 953.
- [5] J.L. Guerriero, *Trends Mol. Med.* 24 (5) (2018) 472.
- [6] T.J. Koh, L.A. DiPietro, *Exp. Rev. Mol. Med.* 13 (2011) e23.
- [7] M. Hesketh, et al., *Int. J. Mol. Sci.* 18 (7) (2017).
- [8] A.E. Boniakowski, et al., *J. Immunol.* 199 (1) (2017) 17.
- [9] L. Zhang, W. Wei, *Pharmacol. Ther.* 207 (2020) 107452.
- [10] Q. Xin, et al., *Life Sci.* 237 (2019) 116925.
- [11] Y. Sun, et al., *Life Sci.* 84 (11–12) (2009) 337.
- [12] X. Chen, et al., *BMC Compl. Alternative Med.* 12 (2012) 254.
- [13] Y. Sun, et al., *Int. Immunopharm.* 24 (2) (2015) 392.
- [14] Z. Ma, et al., *Int. Immunopharm.* 38 (2016) 377.
- [15] T. Zhang, et al., *Biosci Trends* 11 (3) (2017) 308.
- [16] Y.X. Shao, et al., *Drug Des. Dev. Ther.* 11 (2017) 3221.
- [17] C.W.t. Shields, et al., *Sci Adv* 6 (18) (2020), eaaz6579.
- [18] J. Guo, et al., *ACS Nano* 14 (4) (2020) 5075.
- [19] J. Guo, et al., *Mol. Canc.* 20 (1) (2021) 10.
- [20] R. Li, et al., *Biomaterials* 168 (2018) 24.
- [21] N.N. Li, et al., *Mater Sci Eng C Mater Biol Appl* 36 (2014) 287.
- [22] K.P. Vercautse, et al., *Bioconjugate Chem.* 8 (5) (1997) 686.
- [23] J. Zhang, et al., *Nat. Commun.* 12 (1) (2021) 1670.
- [24] J. Gan, et al., *Biomaterials* 219 (2019) 119340.
- [25] K. Izumi, et al., *Nat. Commun.* 6 (2015) 6748.
- [26] X. Qin, et al., *Macromol. Biosci.* 18 (7) (2018), e1800047.
- [27] Z. Yu, et al., *ACS Nano* 14 (4) (2020) 4816.
- [28] Y. Gao, et al., *Int. J. Mol. Sci.* 20 (15) (2019), 3722.
- [29] S. Wang, et al., *J. Inflamm.* 18 (1) (2021) 21 (Lond).
- [30] M.F.P. Graca, et al., *Carbohydr. Polym.* 241 (2020) 116364.
- [31] S.A. Eming, et al., *Sci. Transl. Med.* 6 (265) (2014) 265sr6.
- [32] L. Canedo-Dorantes, M. Canedo-Ayala, *Int. J. Inflamm.* 2019 (2019) 3706315.
- [33] K.M. Vannella, T.A. Wynn, *Annu. Rev. Physiol.* 79 (2017) 593.
- [34] S. Gordon, *Nat. Rev. Immunol.* 3 (1) (2003) 23.
- [35] P.K. Barman, T.J. Koh, *Front Cell Dev Biol* 8 (2020) 528.
- [36] P. Yang, et al., *J. Cell Sci.* 133 (19) (2020), jcs235838.
- [37] R. He, et al., *Mol. Immunol.* 90 (2017) 42.
- [38] L. Cheng, et al., *Research* 2020 (2020) 4907185 (Wash D C).
- [39] S. Vaccari, et al., *Eng Reg* 2 (2021) 1.
- [40] X. Feng, et al., *Eng Reg* 2 (2021) 57.
- [41] M. Oksdath Mansilla, et al., *BMC Biomed Eng* 3 (1) (2021) 6.
- [42] K.L. Aya, R. Stern, *Wound Repair Regen.* 22 (5) (2014) 579.
- [43] H. Yang, et al., *ACS Appl Bio Mater* 4 (2021) 311.
- [44] P. Wang, et al., *Acta Biomater.* 100 (2019) 191.
- [45] H. Ying, et al., *Mater Sci Eng C Mater Biol Appl* 101 (2019) 487.
- [46] Y. Yang, et al., *Trends Pharmacol. Sci.* 41 (10) (2020) 701.
- [47] A.E. Louiselle, et al., *Transl. Res.* 236 (2021) 109–116.
- [48] S.Y. Kim, M.G. Nair, *Immunol. Cell Biol.* 97 (3) (2019) 258.
- [49] E. Everitt, N. Mathioudakis, *Ann. N. Y. Acad. Sci.* 1411 (1) (2018) 153.